Article:
Zeng, Y, Liang, G, Qiang, B et al. (11 more authors) (2018) Terahertz emission from localized modes in one-dimensional disordered systems. Photonics Research, 6 (2). pp. 117-122. ISSN 2327-9125

https://doi.org/10.1364/PRJ.6.000117

Terahertz Emission from Localized Modes in One-Dimensional Disordered Systems

Yongquan Zeng,[1] Guozhen Liang,[1] Bo Qiang,[1] Bo Meng,[1] Hou Kun Liang,[2] Shampy Mansha,[3] Jianping Li,[4] Zhaohui Li,[5] Lianhe Li,[6] Alexander Giles Davies,[6] Edmund Harold Linfield,[6] Ying Zhang,[2] Yidong Chong,[3] and Qi Jie Wang[1,3,*]

[1]*Centre for OptoElectronics and Biophotonics, School of Electrical and Electronic Engineering, Nanyang Technological University, 50 Nanyang Avenue, Singapore, Singapore 639798*
[2]*Singapore Institute of Manufacturing Technology, 2 Fusionopolis Way, Singapore 138634, Singapore*
[3]*School of Physical and Mathematical Sciences, Nanyang Technological University, 21 Nanyang Link, Singapore 637371, Singapore*
[4]*Institute of Photonics Technology, Jinan University, Guangzhou 510632, China*
[5]*State Key Laboratory of Optoelectronic Materials and Technologies, School of Electronics and Information Technology, Sun Yat-sen University, Guangzhou 510275, China*
[6]*School of Electronic and Electrical Engineering, University of Leeds, Woodhouse Lane, Leeds LS2 9JT, U.K.*
**Corresponding author: qjwang@ntu.edu.sg*

Received Month X, XXXX; revised Month X, XXXX; accepted Month X, XXXX; posted Month X, XXXX (Doc. ID XXXXX); published Month X, XXXX

We demonstrate terahertz (THz) frequency laser emission around 3.2 THz from localized modes in one-dimensional (1D) disordered grating systems. The disordered structures are patterned on top of the double-metal waveguide of a THz quantum cascade laser. Multiple emission peaks are observed within a frequency range corresponding to the bandgap of a periodic counterpart with no disorder, indicating the presence of mode localization aided by Bragg scattering. Simulations and experimental measurements provide strong evidence for the spatial localization of the THz laser modes. © 2017 Chinese Laser Press

OCIS codes: 290.4210 Multiple scattering; 040.2235 Far infrared or terahertz; 140.5965 Semiconductor lasers, quantum cascade.

1. INTRODUCTION

The scattering and diffusion of light in disordered media has attracted considerable research interest for many years. One of the reasons for this is the possibility of forming spatially complex localized optical modes [1–5], which can serve as the basis for strongly multi-mode random lasers. Light localization in disordered media arises from an interplay of two effects: Bragg scattering (akin to the effects of a photonic bandgap in a periodic medium), and Anderson localization due to the interference of randomly-scattered waves. A wide range of applications based on the localization of light have been proposed, such as compact and low-threshold lasers, bright light sources with low spatial coherence, wavelength filters, optical switches, sensors [6] and the study of cavity quantum electrodynamics [7].

Terahertz (THz) frequency technology has been a highly topical research field in recent years. Notable achievements include the demonstration and development of THz quantum cascade lasers (QCLs) [8–10], sensitive THz photodetectors [11,12], and THz modulators [13,14]. THz QCLs are electrically-pumped semiconductor lasers exploiting electronic transitions between the subbands of a quantum well superlattice [8]. THz QCLs with various one/two-dimensional designs, including periodic structures [15], graded structures [16,17] and quasi-periodic structures [18,19], have been developed to enable specific functionalities, such as the control of output frequency and beam profiles. However, owing to the long-range distributed feedback mechanism in most of these structures, they possess electromagnetic field distributions that are extended, rather than localized. Random structures [20], however, are a promising method to achieve localized THz modes. Recently, a two-dimensional THz QCL with spatially-confined modes has been demonstrated by fabricating randomly distributed high-index dielectric pillars embedded into low-index polymer background material [21]. The mode localization was enabled by the strong multiple scattering of the dielectric pillars. Nevertheless, the fabrication process was complicated, requiring a polymer planarization process. A simpler alternative route to realize localization is to use a lower-dimensional medium, owing to the reduced number of dimensions for efficient optical feedback [22]. It is known, for instance, that one-dimensional (1D) lattices tend to have much shorter localization lengths than two- or three-dimensional (2D, 3D) lattices.

In this work, we report THz multimode lasing emission around 3.2 THz in a QCL with a 1D disordered grating, comprising subwavelength scatterers with an average spacing on the scale of a quarter-wavelength. A statistical study of the influence of the degree of disorder on the photonic bandgap (PBG) and average gain threshold of the eigenmodes illustrates the localization mechanism.

Spectral measurement and numerical analysis provide evidence for the spatial localization of light.

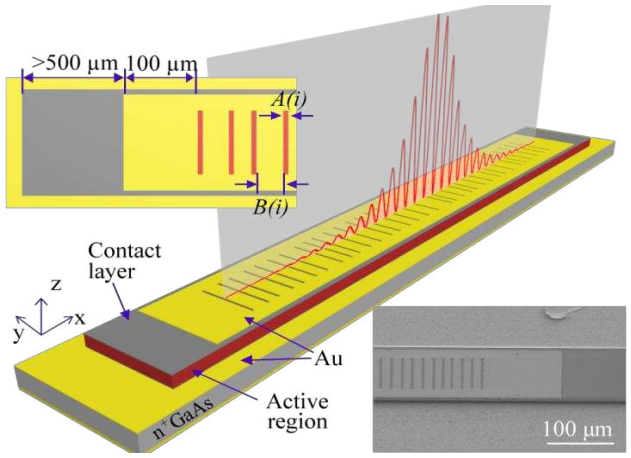

FIG. 1. Schematic diagram of the THz QCL structure with a 1D disordered grating. Insets: top view of the device (top-left), and scanning electron microscope (SEM) image of the fabricated QCL with disordered grating (bottom-right); here the aperture width is 3.5 μm and the disorder degree is 0.2.

2. STRUCTURE DESIGN

Our methodology for implementing the 1D disordered structure is illustrated in Fig. 1. A double-metal ridge waveguide comprising a 10-μm-thick THz quantum cascade active region and a thin (~ 75 nm) heavily-doped top contact layer was fabricated by conventional THz QCL fabrication techniques [23]. Through a lift-off process, slits were created in the top metal plate for laser output, forming an irregular grating. The width of the waveguide and top metal plate are 100 μm and 90 μm respectively, with absorbing boundaries to suppress high-order lateral modes [15]. The total length of the grating is 2 mm, ending with 100 μm wire bonding areas and long absorbing sections (> 500 μm) to eliminate the facet reflection at the two ends of the ridge waveguide. Therefore, the whole structure is a single-lateral-mode waveguide, and the feedback is entirely provided by the multiple scattering from the grating. The widths of the low-index apertures (A) and high-index metal-dielectric-metal (MDM) regions (B) are $A(i) = a$ μm, $B(i) = (14\text{-}a)*(1+\delta)$ μm. Here, i is the period number, a is a constant value, and δ is a random number uniformly distributed between $-\Delta d$ and Δd, where the parameter Δd represents the amount of disorder.

3. RESULTS AND DISCUSSION

A. Optical Property of Disordered Structures

QCLs are electrically pumped, and emit in the transverse-magnetic (TM) polarization owing to the inter-subband selection rules [24]. For THz QCLs in a double-metal ridge waveguide, the subwavelength vertical confinement of the TM mode leads to an impedance mismatch between the areas with and without metal coverage [25]. The effective refractive index contrast of the gratings is estimated to be 2.52:3.50, by calculating the electric field distributions of the fundamental propagating mode in the waveguide at 3.2 THz.

For disordered structures, statistical studies are usually adopted to extract the ensemble-averaged wave propagation properties [26–29]. In this work, to obtain a qualitative understanding of the influence of disorder on the PBG, we use a transfer matrix method to calculate the ensemble-averaged transmission spectra for waveguides with disorder parameters ranging from $\Delta d = 0.0$ to $\Delta d = 0.5$. In the simulation, the 3D disordered waveguide structure

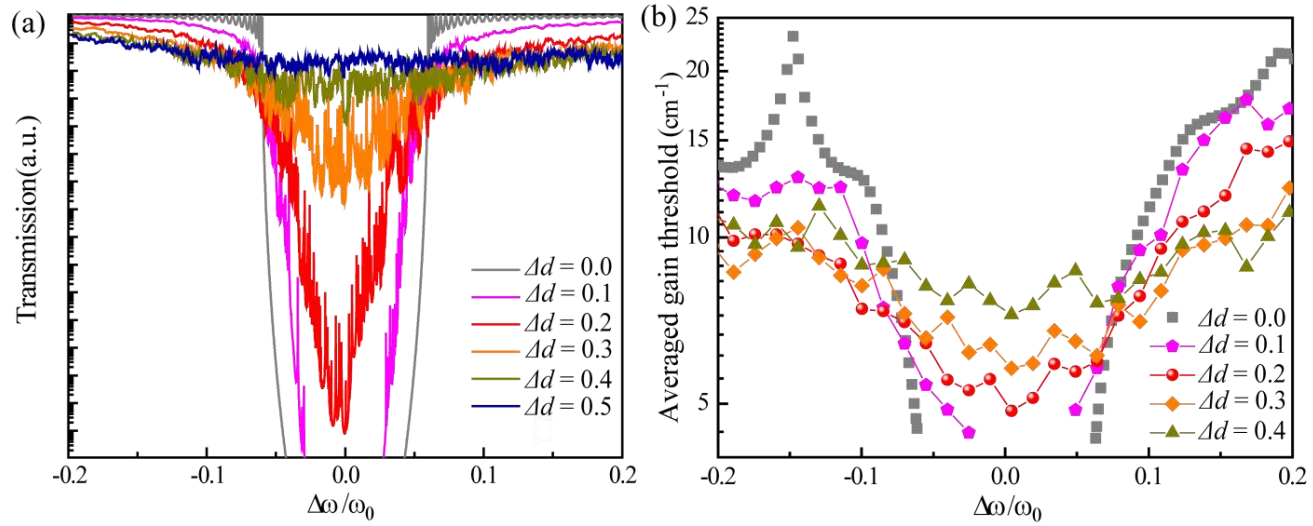

FIG. 2. (a) Ensemble-averaged transmission spectrum over 100 different configurations of the 1D disordered gratings for each degree of disorder. In the simulation, the 3D disordered waveguide structure was simplified to a 1D grating using an estimated refractive index contrast, and without considering waveguide or material loss. (b) Ensemble-averaged gain threshold, calculated from 20 different configurations for each degree of disorder, and taking the mean gain threshold at each frequency bin. The simulation was simplified to a 2D calculation of the structural cross sections where the x-z plane was considered, while the grating was assumed to be infinite in the y direction. For $\Delta d = 0.0$, the peak at $\Delta\omega/\omega_0 = -0.15$ is induced by resonance with the wire bonding areas. This resonance is disrupted and therefore disappears when disorder is introduced. The free carrier absorption losses of the active material were not considered.

was simplified to a 1D grating using the estimated refractive index contrast, without considering active material losses. The transmission spectra were averaged over 100 different configurations for each value of Δd. As shown in Fig. 2a, for the periodic structure, a clear PBG ($\Delta\omega/\omega_0 \sim 0.12$) exists. When disorder is introduced (Δd = 0.1), the transmission gap gets narrower and shallower, while the transmission at the passband decreases. With this degree of disorder, a clear transmission gap still persists, indicating a strong Bragg scattering effect. For the spectrum with Δd = 0.2, the complete PBG disappears. In the individual spectra, multiple narrow transmission peaks are observed to arise within the original PBG range, which are related to the resonant modes induced by the remaining order. For larger values of Δd, the order is even weaker. The gap reduces to a shallow transmission dip and eventually disappears ($\Delta d \sim 0.5 - 0.6$). This indicates that the Bragg scattering is completely disrupted and replaced by random scattering. From the transmission spectra, it can also be concluded that the optical density of states within the original PBG spectral range increases with larger disorder.

From the transmission calculations, it can be inferred that disorder can induce a narrowing and shallowing of the PBG and the emergence of multiple transmission peaks, indicating the increase of optical states inside the original PBG range. However, these results do not provide information about which disorder degree is preferable for realizing multimode random lasing. For this, it is necessary to study the eigenmode properties of the disordered photonic crystal structures. Finite-element-method (FEM) simulations of the 1D grating systems were thus performed using the commercial software Comsol Multiphysics. As a full-structure 3D simulation is time- and memory-consuming, the simulation was simplified to a 2D calculation of the structural cross sections where the x-z plane was considered, while the grating was assumed to be infinite in the y direction. The losses of the active region material were not considered. From the calculated complex eigenfrequency $\omega_r + i\,\omega_i$, the gain threshold to compensate for eigenmode loss can be estimated to be $2n_{eff}\omega_i/c$, where n_{eff} is the modal effective refractive index and c is the velocity of light in vacuum. The ensemble-averaged gain threshold was calculated from 20 different configurations at each disorder degree, taking the mean gain threshold at each frequency bin. Given the peak gain coefficient of THz quantum cascade active region is around 30 cm^{-1}, and the active material loss is around 10 cm^{-1}, only the modes with gain threshold smaller than 20 cm^{-1} offer the prospect for lasing, and are included in the average calculations.

As shown in Fig. 2b, as the disorder parameter is increased from Δd = 0.1 to Δd = 0.4, the optical gap becomes narrower and the ensemble-averaged gain threshold increases continuously. In the pass band, the ensemble-averaged gain threshold first decreases and then fluctuates around a certain level. When Δd = 0.1, Bragg scattering dominates the feedback as an optical gap exists, and the gain threshold of eigenmodes in the pass band correlates with the overall behaviour of the periodic structure. Inside the PBG region, low-threshold modes induced by weak disorder appear. These modes are similar to defect modes in a photonic crystal, and are exponentially localized primarily due to the PBG. By contrast, the electric profiles of eigenmodes in the passband are all extended. With increasing disorder (Δd = 0.2), however, more localized modes appear in the PBG region and the threshold is slightly higher owing to a stronger disorder perturbation. For large disorder (e.g. Δd = 0.4), the effect of random scattering dominates the feedback mechanism. The electric profiles of the eigenmodes, outside the frequency range of the original PBG, exhibit large, random amplitude fluctuations [29] and the average gain threshold decreases to around 10 cm^{-1}. Inside the frequency range corresponding to the original PBG, even more eigenmodes appear but the average gain threshold increases such that the dip induced by Bragg scattering is barely observable.

We estimated the optical localization lengths by [30],

$$L_c = \left(\int \mathrm{abs}(E_z)\,dx\right)^2 \Big/ \int (E_z)^2\,dx \qquad (1)$$

for the localized eigenmodes inside the original PBG. For Δd = 0.1 and 0.2, the optical localization lengths are typically in the range 300 μm to 450 μm, much smaller than the system size. However, the optical localization lengths almost double for Δd = 0.4. This indicates that smaller values of Δd are more favorable for achieving well-localized modes. However, the number of eigenmodes inside the PBG region is larger for stronger disorder. Therefore, disordered grating structures with Δd = 0.2 are chosen for experimental demonstrations, a compromise between having a reasonable number of eigenmodes and a low gain threshold with short localization lengths.

B. Electrical and Optical Characterization

The THz QCL active region used in this work was based on a three-well resonant-phonon design with GaAs/$Al_{0.15}Ga_{0.85}As$ heterostructure active layers [31]. The center of the gain spectrum continuously shifts from 3.05 THz to 3.20 THz with increasing pumping intensity [21]. The dynamic range for a ridge laser of size 2.2 mm × 102 μm is

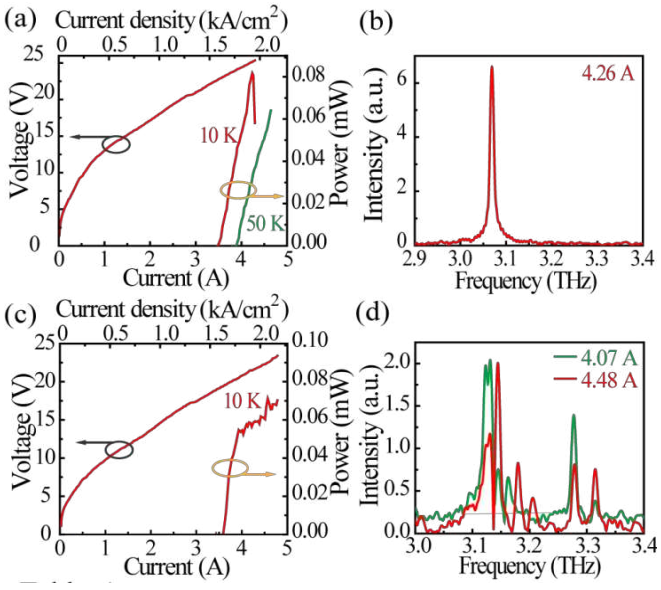

FIG. 3. (a) The light-current-voltage (LIV) curves and (b) emission spectrum at 4.26 A for the fabricated 1D periodic QCL. (c) The LIV curve and (d) emission spectra for the fabricated 1D disordered QCL with Δd = 0.2. The emission spectra were measured at a heat-sink temperature of 10 K with a resolution of 0.2 cm^{-1}. The aperture width of the devices is 3.5 μm.

~ 1.3 kA/cm² to 2.3 kA/cm². As the gain spectral range is smaller than the bandgap size of the periodic structure, the lower band edge was located within this frequency regime. The fabricated QCLs have 1D gratings with three typical disorder degrees, i.e. perfectly periodic distribution (Δd = 0.0), moderate disorder distribution (Δd = 0.2) and strong disorder distribution (Δd = 0.6). The emission spectra of the fabricated devices were captured using a Fourier-transform infrared spectroscopy system (Vertex 70v, Bruker) with a room-temperature deuterated triglycine sulfate detector. The scanning resolution was set to be 0.2 cm^{-1}. The devices were driven by an electrical pulse generator with a repetition rate of 10 kHz and a pulse width of 500 ns.

Fig. 3 shows the light-current-voltage (LIV) curves and the corresponding emission spectra of the QCLs with a periodic grating (Δd = 0.0) and a disordered grating (Δd = 0.2). The threshold current density of the periodic grating laser is around 1.58 kA/cm² at 10 K. A stable single mode was observed at 3.07 THz for the whole dynamic range, even though the gain spectrum center shifts with increasing pumping current. This indicates the position of the lower band edge. For the disordered QCL with Δd = 0.2, the threshold current density at 10 K is 1.79 kA/cm², slightly higher than that of the periodic counterpart. More than eight peaks are present in its emission spectrum, with frequencies located inside the PBG of the original periodic gratings (the peak frequencies and the corresponding thresholds are listed in Table.1). The multiple peaks appear almost simultaneously, indicating that the corresponding mode thresholds are approximately equal. The emission peaks should correspond to the predicted localized modes of the disordered grating system. For the QCL with highly-disordered gratings (not shown), the threshold current density is much higher and the number of peaks is limited (normally to two peaks). This is attributed to the large gain threshold induced by the breakdown of Bragg scattering and the delocalization of eigenmodes.

Freq. (THz)	3.123	3.131	3.145	3.160	3.181	3.204	3.279	3.315
Thres. (A)	3.624	3.716	3.812	3.624	4.305	4.421	3.656	4.069

Table 1. The peak frequencies (THz) and the corresponding lasing threshold currents (A) corresponding to the spectra in Fig. 3d.

C. Mode localization

Near-field scanning optical microscopy (NSOM) can be used for direct observation of the mode profile. Unfortunately, it cannot normally be used at very low temperatures unless a dedicated cryocooling system is designed [32]. We thus adopted the following alternative method to verify the localization of the lasing modes.

If a lasing mode is localized near the center of a grating, the threshold should be largely insensitive to changes at the boundaries. Therefore, the sensitivity of a mode threshold can be used to determine its field distribution indirectly. We fabricated two different sets of disordered gratings in series on the same ridge, with a disorder degree Δd = 0.2. The gap between the two sets of gratings is 30 μm, as shown in Fig. 4a. When one of the gratings (referred to

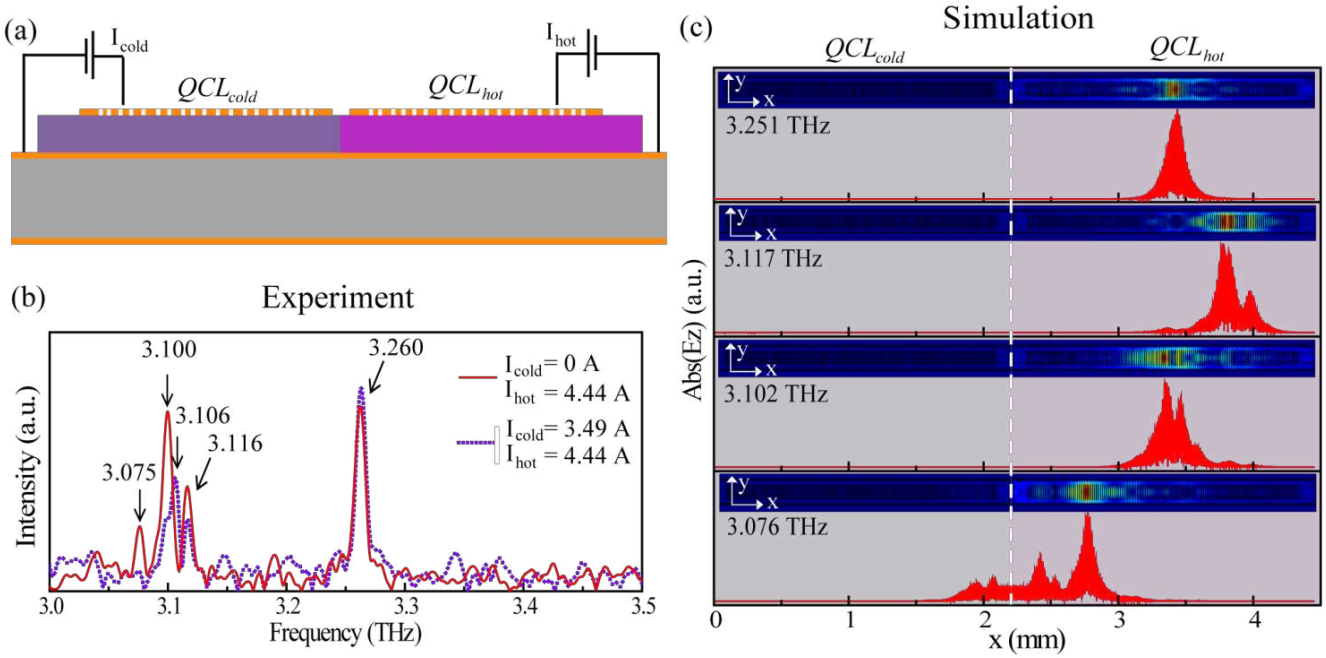

FIG. 4. (a) A schematic diagram showing two different sets of disordered gratings with disorder degree of Δd = 0.2 fabricated on the same ridge, with the two lasers being pumped separately. (b) The emission spectra under different pumping conditions. The peaks are labelled by the frequency value in THz. (c) The calculated mode distributions (red curves) corresponding to four emission peaks when the "cold" laser was not pumped. The simulation was simplified to a 2D calculation of the structural cross sections where the x-z plane was considered, while the grating was assumed to be infinite in the y direction. For the cold laser, imag($n_{GaAs/AlGaAs}$) = -0.01i; whilst for the hot laser, imag($n_{GaAs/AlGaAs}$) = 0.01i. Inset: field distribution snapshots of the top-view structure calculation (x-y plane within the active region, as shown in Fig. 1). The calculation results for cross section (red curves) and top view (field distribution snapshots) of the same structure agree well.

here as the "hot laser") is electrically pumped above threshold, the generated light will be absorbed by the 30 μm gap and the other passive device (the "cold" laser). If the cold laser is also pumped, the optical loss through the boundary of the hot laser will be reduced. At a pump current of 4.44 A, the hot laser has four emission peaks, as shown in Fig. 4b (red curve). When the cold laser is pumped with a small current, the thresholds of all four peaks of the hot laser undergo no obvious change. When the pump current of the cold laser is increased but still remains below the lasing threshold of the cold laser, the mode at 3.075 THz is greatly suppressed and another mode (3.106 THz) appears, indicating that the tail of 3.075 THz mode extends into the cold laser region. The new mode may correspond to a higher order lateral mode in the same region, with its emergence being due to greatly reduced optical losses when the cold laser is pumped. In contrast, the threshold currents of the other three peaks remain largely unchanged. This indicates that the mode corresponding to the peak at 3.075 THz is located quite close to the left boundary, while the other three modes (3.100 THz, 3.116 THz, and 3.260 THz) are localized away from this boundary. In 2D simulations of the structure, shown in Fig. 4c, the calculated eigenmode field distributions with the lowest gain thresholds qualitatively confirm this interpretation (there is a slight frequency discrepancy, which can be attributed to imperfections in the simulation models).

Further evidence for mode localization was found by covering half of the surface of a disordered laser (for which characteristics were reported in Fig. 3c and 3d) with a copper sheet whilst measuring the emission spectrum [21]. The copper sheet was fixed at a distance of ~ 1 mm above the device surface, and emission spectra were then compared without (red curve) and with (violet dashed curve) the copper sheet in place. It was observed that the emission intensity of peaks at 3.127 THz and 3.164 THz (brown dashed arrows) underwent no obvious change with the copper covering. Therefore, these modes are located in the uncovered region. The intensity of emission peak at 3.146 THz (black solid arrow) was, however, reduced, implying that the emission was partially blocked. Furthermore, the emission peaks at 3.133 THz and 3.283 THz (blue solid arrows) was completely suppressed, implying that they were totally blocked by the copper sheet. An attempt to measure the emission at different angles was also made by modulating the position of the device with the copper covering. But there was still no emission observed at these two frequencies, indicating that the modes were located totally within the covered region. Spectra measured at different currents also showed a similar behaviour, indicating the stability of the field distributions. Furthermore, when the copper sheet was removed, all peaks returned to their original intensities, confirming the robustness of the measurements. From the above observations, we may conclude that the emission modes of 1D disordered QCL are localized.

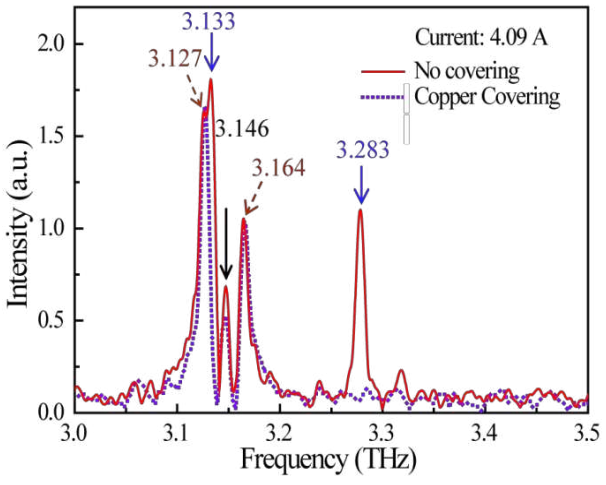

Fig. 5. The emission spectra of a 1D disordered QCL without (red curve) and with (violet dashed curve) partial covering by a copper sheet. The pumping current is 4.09 A. All the peaks are labelled by their frequency values in THz. The arrows are referred to in the text.

4. CONCLUSIONS

In conclusion, we have developed 1D THz frequency QCLs with disordered gratings that support multiple localized lasing modes. The modes occur in the frequency range predicted by numerical models. Evidence for mode localization is provided by numerical and experimental analyses. This ability to form multiple localized modes, with simultaneous emission over a band of frequencies, may find applications in the development of speckle-free imaging and multi-wavelength spectroscopy.

Acknowledgement. Funding support is acknowledged from the Singapore Ministry of Education Tier 2 Program (MOE 2016-T2-1-128); Agency for Science, Technology and Research (A*STAR) (Grant No. 1426500050); the Singapore National Research Foundation Competitive Research Program (NRF-CRP18-2017-02); and, the UK Engineering and Physical Sciences Research Council (EP/P021859/1). We also acknowledge the support of the Royal Society and Wolfson Foundation.

Reference

1. H. Cao, J. Y. Xu, D. Z. Zhang, S. H. Chang, S. T. Ho, E. W. Seelig, X. Liu, and R. P. H. Chang, "Spatial confinement of laser light in active random media," Phys. Rev. Lett. **84**, 5584–5587 (2000).
2. P. Sebbah and C. Vanneste, "Random laser in the localized regime," Phys. Rev. B **66**, 1–10 (2002).
3. J. Fallert, R. J. B. Dietz, J. Sartor, D. Schneider, C. Klingshirn, and H. Kalt, "Co-existence of strongly and weakly localized random laser modes," Nat. Photonics **3**, 279–282 (2009).
4. A. Consoli, D. Mariano, N. U. Wetter, and C. López, "Large area resonant feedback random lasers based on dye-doped biopolymer films," Opt. Express **23**, 303–310 (2015).
5. A. Consoli and C. Lopez, "Emission regimes of random lasers with spatially localized feedback," Opt. Express **24**, 10912 (2016).

6. D. S. Wiersma, "Disordered photonics," Nat. Photonics **7**, 188–196 (2013).
7. L. Sapienza, H. Thyrrestrup, S. Stobbe, P. D. Garcia, S. Smolka, and P. Lodahl, "Cavity quantum electrodynamics with Anderson-localized modes," Science **327**, 1352–1355 (2010).
8. R. Kohler, A. Tredicucci, F. Beltram, H. E. Beere, E. H. Linfield, A. G. Davies, D. A. Ritchie, R. C. Iotti, and F. Rossi, "Terahertz semiconductor-heterostructure laser," Nature **417**, 156–159 (2002).
9. B. S. Williams, "Terahertz quantum-cascade lasers," Nat. Photonics **1**, 517–525 (2007).
10. G. Liang, T. Liu, Q. J. Wang, and S. Member, "Recent Developments of Terahertz Quantum Cascade Lasers," IEEE J. Sel. Top. Quantum Electron. **23**, (2017).
11. H. C. Liu, C. Y. Song, A. J. SpringThorpe, and J. C. Cao, "Terahertz quantum-well photodetector," Appl. Phys. Lett. **84**, 4068–4070 (2004).
12. M. Graf, G. Scalari, D. Hofstetter, J. Faist, H. Beere, E. Linfield, D. Ritchie, and G. Davies, "Terahertz range quantum well infrared photodetector," Appl. Phys. Lett. **84**, 475–477 (2004).
13. B. Sensale-Rodriguez, R. S. Yan, M. M. Kelly, T. Fang, K. Tahy, W. S. Hwang, D. Jena, L. Liu, and H. G. Xing, "Broadband graphene terahertz modulators enabled by intraband transitions," Nat. Commun. **3**, 780 (2012).
14. G. Liang, X. Hu, X. Yu, Y. Shen, L. H. Li, A. G. Davies, E. H. Linfield, H. K. Liang, Y. Zhang, and S. F. Yu, "Integrated Terahertz Graphene Modulator with 100% Modulation Depth," ACS Photonics **2**, 1559–1566 (2015).
15. Y. Chassagneux, R. Colombelli, W. Maineult, S. Barbieri, H. E. Beere, D. a Ritchie, S. P. Khanna, E. H. Linfield, and a G. Davies, "Electrically pumped photonic-crystal terahertz lasers controlled by boundary conditions.," Nature **457**, 174–178 (2009).
16. G. Liang, H. Liang, Y. Zhang, S. P. Khanna, L. Li, A. G. Davies, E. Linfield, D. F. Lim, C. S. Tan, S. F. Yu, H. C. Liu, and Q. J. Wang, "Single-mode surface-emitting concentric-circular-grating terahertz quantum cascade lasers," Appl. Phys. Lett. **31119**, (2013).
17. G. Liang, H. Liang, Y. Zhang, L. Li, and A. G. Davies, "Low divergence single-mode surface-emitting concentric-circular-grating terahertz quantum cascade lasers," Opt Express **21**, 586–590 (2013).
18. L. Mahler, A. Tredicucci, F. Beltram, C. Walther, J. Faist, H. E. Beere, D. A. Ritchie, and D. S. Wiersma, "Quasi-periodic distributed feedback laser," Nat. Photonics **4**, 165–169 (2010).
19. M. S. Vitiello, M. Nobile, A. Ronzani, A. Tredicucci, F. Castellano, V. Talora, L. Li, E. H. Linfield, and A. G. Davies, "Photonic quasi-crystal terahertz lasers," Nat. Commun. **5**, (2014).
20. S. Schönhuber, M. Brandstetter, T. Hisch, C. Deutsch, M. Krall, H. Detz, A. M. Andrews, G. Strasser, S. Rotter, and K. Unterrainer, "Random lasers for broadband directional emission," Optica **3**, 1035 (2016).
21. Y. Zeng, G. Liang, H. K. Liang, S. Mansha, B. Meng, T. Liu, X. Hu, J. Tao, L. Li, A. G. Davies, E. H. Linfield, Y. Zhang, Y. Chong, and Q. J. Wang, "Designer Multimode Localized Random Lasing in Amorphous Lattices at Terahertz Frequencies," ACS Photonics **3**, 2453–2460 (2016).
22. E. Abrahams, P. W. Anderson, D. C. Licciardello, and T. V. Ramakrishnan, "Scaling theory of localization: Absence of quantum diffusion in two dimensions," Phys. Rev. Lett. **42**, 673–676 (1979).
23. B. S. Williams, S. Kumar, H. Callebaut, Q. Hu, and J. L. Reno, "Terahertz quantum-cascade laser at lambda approximate to 100 μm using metal waveguide for mode confinement," Appl. Phys. Lett. **83**, 2124–2126 (2003).
24. J. Faist, F. Capasso, D. L. Sivco, C. Sirtori, A. L. Hutchinson, and A. Y. Cho, "Quantum Cascade Laser," Science **264**, 553–556 (1994).
25. S. Kumar, B. S. Williams, Q. Qin, A. W. M. Lee, and J. L. Reno, "Surface-emitting distributed feedback terahertz quantum-cascade lasers in metal-metal waveguides," **15**, 113–128 (2007).
26. V. D. Freilikher, B. A. Liansky, I. V Yurkevich, A. A. Maradudin, and A. R. Mcgurn, "Enhanced transmission due to disorder," Phys. Rev. E **51**, 6301–6304 (1995).
27. L. I. Deych, D. Zaslavsky, and A. A. Lisyansky, "Statistics of the Lyapunov exponent in 1D random periodic-on-average systems," Phys. Rev. Lett. **81**, 5390–5393 (1998).
28. S. H. Chang, H. Cao, and S. T. Ho, "Cavity formation and light propagation in partially ordered and completely random one-dimensional systems," IEEE J. Quantum Electron. **39**, 364–374 (2003).
29. K. Y. Bliokh, Y. P. Bliokh, and V. D. Freilikher, "Resonances in one-dimensional disordered systems: localization of energy and resonant transmission," J. Opt. Soc. Am. B **21**, 113–120 (2004).
30. T. Schwartz, G. Bartal, S. Fishman, and M. Segev, "Transport and Anderson Localization in two-dimensional photonic lattices," Nature **446**, 52–55 (2007).
31. M. Belkin, Q. Wang, C. Pflügl, A. Belyanin, S. P. Khanna, A. G. Davies, E. H. Linfiel, and F. Capasso, "High-temperature operation of terahertz quantum cascade laser sources," IEEE J. Sel. Top. Quantum Electron. **15**, 952–967 (2009).
32. I. C. Moldovan-Doyen, G. Xu, L. Greusard, G. Sevin, E. Strupiechonski, G. Beaudoin, I. Sagnes, S. P. Khanna, E. H. Linfield, A. G. Davies, R. Colombelli, and Y. De Wilde, "Low temperature near-field scanning optical microscopy on infrared and terahertz photonic-crystal quantum cascade lasers," Appl. Phys. Lett. **98**, 96–98 (2011).